A hundred year record of industrial and urban development in French Alps combining Hg accumulation rates and isotope composition in sediment archives from Lake Luitel

Stéphane Guédron, David Amouroux, Pierre Sabatier, Carole Desplanquee, Anne-Lise Develle, Julien P. G. Barre, Caiyan Feng, Frédéric Guiter, Fabien Arnaud, Jean-Louis Reyss, et al.

A hundred year record of industrial and urban development in French Alps combining Hg accumulation rates and isotope composition in sediment archives from Lake Luitel

Stéphane Guédron, David Amouroux, Pierre Sabatier, Carole Desplanque, Anne-Lise Develle, Julien Barre, Caiyan Feng, Frederic Guiter, Fabien Arnaud, Jean Louis Reyss, Laurent Charlet

PII:
DOI: doi: 10.1016/j.chemgeo.2016.03.016
Reference:

To appear in:

Received date: 5 December 2014
Revised date: 24 February 2016
Accepted date: 15 March 2016

A hundred year record of industrial and urban development in French Alps combining Hg accumulation rates and isotope composition in sediment archives from Lake Luitel.

Stéphane Guédron [a]*, David Amouroux [b], Pierre Sabatier [c], Carole Desplanque [e], Anne-Lise Develle [c], Julien Barre [b], Caiyan Feng [b], Frederic Guiter [d], Fabien Arnaud[c], Jean Louis Reyss [f] and Laurent Charlet [a].

[a] Institut des Sciences de la Terre (ISTerre), University Grenoble-Alpes, Institut de Recherche pour le Developpement (IRD) – UMR 5275 (IRD/UJF/CNRS) – BP 53, F-38041 Grenoble, France

[b] LCABIE - Laboratoire de Chimie Analytique Bio-Inorganique et Environnement, IPREM UMR 5254, CNRS et Université de Pau et des Pays de l'Adour, Hélioparc, F-64053 Pau, France

[c] Environnement, Dynamique et Territoires de Montagne (EDYTEM), Université Savoie Mont Blanc, CNRS, 73373 Le Bourget du Lac, France.

[d] Institut Méditerranéen de Biodiversité et d'Ecologie marine et continentale (IMBE), UMR 7263 CNRS IRD, Aix-Marseille University, Avignon University(Technopôle de l'Arbois BP 80, 13545 Aix-en-Provence cedex 04, France)

[e] Office National des Forêts, 9 quai Créqui, 38000 Grenoble, France.

[f] Laboratoire des Sciences du Climat et de l'Environnement, Université de Versailles Saint-Quentin CEA-CNRS, avenue de la terrasse, 91198 Gif-sur-Yvette cedex, France.

* Corresponding author

E-mail: stephane.guedron@ird.fr

Tel : +33 (0)4-76-63-59-28

Fax : + 33 (0)4-76-63-52-52

Abstract:

This study reconstructs the history of multiple industrial and urban mercury (Hg) emissions recorded in the sediment archive of Lake Luitel (France) from AD ~1860 to AD 2011. For this purpose, we provide a well constrained short-lived radionuclides continuous age – depth relationship of the sediment sequence (mean accumulation rate of 5.18 ± 0.28 $mm.yr^{-1}$) with Hg accumulation rates (Hg AR), Hg isotopic composition and extensive historical data. Hg AR were stable around 45 $\mu g.m^{-2}.y^{-1}$ from 1860 to WWI and rose to reach their maximum at the end of WWII (250 $\mu g\ m^{-2}\ y^{-1}$) followed by a gradual decreased to reach about 90 $\mu g\ m^{-2}\ y^{-1}$ in the current period. Normalization to a terrigenous Hg proxy highlighted the dominance of atmospheric Hg inputs to the lake. The combination of Hg AR with isotopic signatures through the use of binary mixing (Δ^{199}Hg vs 1/Hg AR) models and isotopic plots (and comparison to literature data) allowed us to identify the main industrial and urban historical inputs. The major outcome of this study is that the Hg mass independent fractionation (MIF) signature did not enable the identification of particular anthropogenic sources but reflected an integrated pool of industrial and urban emissions which tend to shift to less negative MIF values (mean: -0.15 ± 0.04 ‰) during their period of maximum emissions. Temporal MIF and Hg AR variations depict the rising Hg emissions from the industrial revolution (1860-1910) to the modern industrial and urban development period (1950 – 1980). Mass dependent fractionation (MDF) signatures enabled the identification of major contributors in relation to their relative intensities lying between two endmember pools: (i) the combustion activities (smelters, cement factories and urban heating) with more negative δ^{202}Hg values, and (ii) the chemical and electrometallurgical activities (electrochemistry, chlor-alkali) with higher δ^{202}Hg values. Unconformities of MIF and MDF signatures were observed during WWI, WWII and interwar period, and were attributed to drastic and rapid changes in regional industrial activities. Finally, recent laws regarding Hg emissions (1998 – 2011) prove their

efficiency as Hg AR decreased with a return to more negative MIF and MDF signatures such as during the industrial revolution period. Our study highlights that the combination of Hg isotopic data with Hg AR in sediment archives is a useful tool for reconstructing the history of anthropogenic Hg emissions, and has the potential to identifiy their relative contributions.

Key words: mercury, isotopes, lake sediment, urban area, industry.

1. Introduction.

The history of atmospheric Hg pollution over the last 3000 years in Europe has been well documented by a variety of studies using lake and lagoon sediments, peat deposits and Greenland or Arctic ice cores as environmental archives (Allan et al., 2013; Elbaz-Poulichet et al., 2011; Jackson et al., 2004; Lamborg et al., 2002; Roos-Barraclough et al., 2002b; Thevenon et al., 2011). The recent development of high precision mass spectrometry tools allows us to go further in the tracking of Hg sources using Hg isotopes as tracers. Indeed, mercury isotopes display large mass dependent (MDF) and mass independent (MIF) fractionation ranges (≈ 7 ‰ for the δ^{202}Hg and ≈ 10 ‰ for the Δ^{199}Hg, respectively) resulting from biophysico-chemical processes taking place either in natural or anthropogenic sources independently (Bergquist and Blum, 2007; Sonke, 2011). In parallel, the use of MIF signatures enables the identification of specific sources (i.e., coal, oil and ores) and certain geochemical processes since the MIF is expected to be unaltered by MDF processes, but can be modified by other MIF processes or through mixing of Hg pools with different MIF signatures (Bergquist and Blum, 2007; Blum et al., 2014a; Blum et al., 2014b; Sonke, 2011; Wiederhold, 2015).

Up to now, few studies have successfully discriminated anthropogenic mercury sources in sediments archives from background sources using Hg isotopes, and followed their distribution and mixing in the environment (Bigham et al., 2013; Donovan et al., 2014; Estrade et al., 2011; Gray et al., 2013; Jackson et al., 2004; Jackson and Muir, 2012; Ma et al., 2013; Mil-Homens et al., 2013; Sonke et al., 2010). It is a challenging approach since recorded MIF and MDF signatures in sediment can result from a mixture of different Hg pools and from numerous processes (including photo-reduction, volatilization and microbial-reduction). Thus, there is a real need to validate the use of this new proxy for the

identification of historical, current, local and global sources of Hg pollution and their transport pathways.

In the surrounding valleys of Lake Luitel located in the French Alps, industry (including (electro)-metallurgy, (electro & organo)-chemistry and cement factories) and urban areas including Grenoble city (with its incinerators, urban heating and automobile traffic) grew rapidly in the early 20th century due to an easy access to hydroelectricity and to the vicinity of coal and metal-ore mines (Figure 1). Both urban and industrial developments have changed the regional landscape and impacted the surrounding environment (Dommergue et al., 2002; Grangeon et al., 2012; Guédron et al., 2013). More recently, environmental regulations were imposed to the urban and industrial sectors in order to reduce their respective atmospheric emissions and improve air quality.

In this study, we used a sedimentary record from Lake Luitel, which is characterized by a high sedimentation rate and a small catchment area enabling to record multiple urban and industrial Hg pollution sources from the surrounding industrial alpine valleys. To reconstruct the history of Hg emissions and sources over the last 150 years, we combined historical information with high resolution Hg accumulation rates, Hg isotopic composition and major and trace elements.

2. Materials and methods

2.1. Description of Lake Luitel

Lake Luitel (N45° 05′ 26″, E 5° 50′ 55″, 1262 m above sea level, surface area = 1.94 ha) is located in the National Natural Luitel Park at the eastern part of Grenoble city in the French Alps (see http://www.reserves-naturelles.org/lac-luitel) in a depression of the crystalline Belledonne range bedrock mainly composed of metamorphic rocks (i.e., mica-schists and amphibolites). The lake color is black, typical of acidic and organic rich water, and it is

encircled by bog type vegetation (i.e., Sphagnum mosses). The Lake water inputs come from rain events and snow melt collected over a small catchment area (309 ha). Lake Luitel freezes for two to four months each year. The main tributary of Lake Luitel is a small river (water flow ~ 10 L s^{-1}) characterized by low conductivity (< 20 µS.cm^{-1}) water (Desplanque and Garambois, 2009). The lakeside has undergone several transformations over time with (i) the displacement of a small road (which bypasses the lake) from the western to the eastern side of the Lake in 1930, (ii) the construction of buildings for local workers (between 1925 to 1943) and (iii) the construction of a main road in 1937, located ~ 50 m to the North of the lake, leading to the Chamrousse ski resort.

2.2. Anthropogenic sources and dominant winds

Lake Luitel is located in-between three industrial valleys (the Romanche Valley, the Isère valley, and the Grenoble City valley at the confluence - Figure 1). In the vicinity of Lake Luitel, the main anthropogenic sources can be classified with respect to their distances from the lake (Figure 1). Close to the lake, in the Romanche valley, the major sources are (i) ferrous and non-ferrous mines which were active during the 19th century and (ii) (electro)-metallurgical factories which are still in activity. Downstream, (iii) chemical industries are located in the South of Grenoble city and (iv) cement factories located further away in the north west of Grenoble city. Dominant winds are North-North-West or South-East (Figure 1) with stable thermic inversion layer mainly during the winter period (Chemel et al., 2005; Milhe et al., 1971; Mimeau, 2013).

2.3. Sediment core collection

Two 80 cm gravity cores (LUI12P1 and LUI1201) were collected in the center of the lake Luitel using a UWITEC corer. Sampling was performed on the frozen lake in February 2012

from a hole drilled in the ice cover. Each of LUI12P1 and LUI1201 cores were split into two halves (S.I.1); one for the X-ray fluorescence (XRF) core scanning analysis and the other one was sub-sampled every 1 cm for chemical and chronological analyses. Total mercury analysis were performed on LUI12P1a core and Hg isotopes analysis were performed on LUI1201a core samples. LUI12P1b and LUI1201a cores were cross correlated with XRF core scanning (SI. 1).

2.4. Chemical analyses

Details for sample preparation and chemical analysis are given in S.I.1. All analytical procedures were conducted using ultra clean techniques (Cossa and Gobeil, 2000). Briefly, XRF analysis was performed on the fresh surfaces of the split sediment cores every 5 mm using a non-destructive Avaatech core-scanner (S.I. 1). Geochemical data were obtained at different tube settings, 10 kV - 2 mA for Al, Si, S, K, Ca, Ti, Mn, Fe and at 30 kV – 0.5 mA for Cu, Zn, Br, Sr, Rb, Zr, Pb (Richter et al., 2006). Total mercury concentrations ([$(THg)_P$]) were determined by combustion and atomic absorption spectrophotometry (S.I. 1) using an AMA 254 analyzer (Altec) (Guédron et al., 2009; Roos-Barraclough et al., 2002a). Hg accumulation rates (AR Hg) were obtained from THg concentration, dry density and age period covered by each slice. Principal Component Analysis (PCA) was conducted with "R" software and provided statistical association between chemical parameters (S.I. 2).

Hg isotopes (S.I. 3) were determined at the LCABIE laboratory after digestion of the sediment sample in 50 mL PE vials with 4 mL of HNO_3/HCl/H_2O_2 mixture (3:1:1) and heated at 85°C for 4 hours according to the procedure established by Foucher and Hintelmann (2006). Then, they were centrifuged at 1400 rpm for 10 min and the supernatant was removed and diluted for isotopic measurements. Hg isotope analyses were performed according to previous methods (Bergquist and Blum, 2007; Gehrke et al., 2009; Lauretta et al., 2001) using

a cold vapor generation with $SnCl_2$ reduction coupled to a MC-ICP-MS (Nu Plasma, Nu Instrument). Raw data for samples and CRMs are provided in S.I.3. To correct the instrumental mass bias, internal standard of Tl (NIST 997, $^{205}Tl/^{203}Tl$ = 2.38714) and sample standard bracketing with NIST 3133 standard solution were used. All samples and standards were analyzed at 1 ppb of Hg. MDF of Hg are reported relative to the NIST 3133 Hg solution (Blum and Bergquist, 2007):

$$\delta^{xxx}Hg = \left(\frac{xxx/^{198}Hg_{sample}}{xxx/^{198}Hg_{NIST\ 3133}} - 1\right) * 1000\ in\ ‰$$

where xxx is the studied isotopes. For ^{199}Hg and ^{201}Hg isotopes, MIF of Hg is reported as the difference between the theoretical value predicted by MDF of $\delta^{199}Hg$ and $\delta^{201}Hg$ and the measured values and noted $\Delta^{199}Hg$ and $\Delta^{201}Hg$ in ‰ (Blum and Bergquist, 2007):

$\Delta^{199}Hg = \delta^{199}Hg - 0.252 \times \delta^{202}Hg$

$\Delta^{201}Hg = \delta^{201}Hg - 0.752 \times \delta^{202}Hg$

Analytical uncertainty was evaluated by multiple measurements of UM-Almadén standard and IAEA 405 (sediment) certified reference material (SI. 3). Values obtained are -0.53 ± 0.16 ‰ and 0.30 ± 0.11‰ for $\delta^{202}Hg$ and -0.04 ± 0.08‰ and -0.01 ± 0.15‰ for $\Delta^{199}Hg$, respectively (2SD for all uncertainty). Throughout the manuscript, individual and mean values and are presented with their associated 2SD.

2.5. Dating

^{210}Pb and ^{137}Cs short-lived radionuclide gamma decay was analyzed at a 1-cm interval over the uppermost 50 cm, using well-type, germanium detectors at the Laboratoire Souterrain de Modane (LSM) following the procedure of Reyss et al. (1995).

3. Results and discussions

3.1. Chronology

Chronological framework was established through short-lived radionuclides (Appleby and Oldfield, 1978; Golberg, 1963). A logarithmic plot of ^{210}Pbex activity shows a general decrease with a well constrained linear trend (Figure 2a and S.I.1).

The constant flux, constant sedimentation rate (CFCS) model (Golberg, 1963; Krishnaswamy et al., 1971) of the ^{210}Pb data indicate a mean accumulation rate of 5.18 ± 0.28 mm.yr^{-1} (at 1 sigma) over the top 50 cm (Figure 2a). In the ^{137}Cs data, the depth of maximum ^{137}Cs activity in the sediment, corresponding to the maximum atmospheric production in 1963 (Robbins and Edgington, 1975), is observed at 28.5 ± 0.5 cm depth (Figure 2b). The onset of significant levels of weapons test fallout in 1954 (Klaminder et al., 2012) is also depicted at 30.5 ± 0.5 cm depth. In the upper part of the core, at 11.5 ± 0.5 cm depth, a second ^{137}Cs peak is observed which corresponds to the Chernobyl accident dated of 1986 (Figure 2b). The good agreement between ages derived from the CFCS model and from artificial radionuclide data provides a well constrained continuous age–depth relationship over the last century (Figure 2c).

3.2. End-member contributions to the sediment using multi-proxies

The principal component analysis of THg and of the total concentration measured for 15 other elements by XRF on bulk sediment (S.I. 2) allowed us to identify four different geochemical end-members (Sabatier et al., 2010), namely (i) Al, K, Fe, Ti, Rb, Si, Zr and Sr; related to terrigenous input from the watershed (alumino-silicate and heavy minerals), (ii) Br; linked to organic matter (OM) in lake sediment (Bajard et al., 2016, in press), (iii) Mn and S; related to redox processes and (iv) Hg and Pb; mainly associated with human activities.

Terrigenous proxies, i.e., Al, K, Fe, Ti, Rb, Si, Zr and Sr (Fig. 3 and S.I. 4) typical of the watershed metamorphic rock weathered products did not show any significant variation from

the base of the core up to 47 cm depth (~ AD 1921). Then, an increase is observed, suggesting a detrital period, followed by a gradual decrease up to 37 cm depth (~ AD 1939). According to age standard deviations (SD) on this period (± 6 years), the detrital period is likely related to the displacement of the nearby main road from the Western to the Eastern side of the lake and to the construction of a new large building for local workers (from 1925 to 1943). During this period, the bordering Eastern part of the lake watershed was deforested, soils were stripped off, ground was flattened (with rubble/backfill) and the course of the stream was changed. Then, from 37 cm up to the top of the core, terrigenous proxies show a gradual decrease which can be attributed to the change in the main stream course that was significantly reduced in proximity of the lake. In addition, the slight gradual increase of Br during this period suggests that OM deposition in the lake increased and thus diluted the detritic depositions.

Elements of atmospheric origin (i.e., Pb and Hg) show a different pattern. Lead, which can originate from both terrigenous and atmospheric sources, exhibits a gradual increase from 52 cm (~ AD 1910) to around 15cm depth (~ late 1980's) followed by a significant decrease to reach the late 1800's values in the most recent samples. Using aluminium (Al) as a tracer of the alumino□silicate fraction (known as the main carrier phase of natural Pb with organic matter (Elbaz-Poulichet et al., 2011)) or Rubidium (Rb), a conservative element in the chemical weathering process, both Al or Rb normalized Pb profiles (Fig. 3 and S.I. 4) show that lake sediments recorded an increasing Pb pollution due to gasoline and incinerators from the late 1950's to the nowadays (Thevenon et al., 2011). However, the growth of the neighboring Grenoble city and its associated car fleet within the vicinity of the nearby main road to access to the ski resort of Chamrousse suggest that leaded gasoline is the likely major source of Pb to the Lake. Similarly to lead, Hg has both terrestrial and atmospheric origins (Guédron et al., 2006). Total mercury concentrations (THg) were close to the local

geochemical background (~ 100 ng g^{-1}) (Guédron et al., 2013) from the base of the core (~ AD 1860) to 50 cm depth (~ AD 1915). Then they gradually increase to reach higher concentrations (377 ng g^{-1}) at 33 cm depth (~ AD 1947). From 33 to 21cm (AD 1947 -1970), Hg concentrations progressively decreased to reach a plateau around 300 ng g^{-1} between 21 and 10 cm depth (AD 1970 □ 1990) followed by a decrease to reach 230 ng g^{-1} at the top of the core (2012). Hg and S were strongly correlated (Figure 3 and S.I.2) in the entire profile according to the main organic nature of the sediment and to the strong affinity of Hg for OM sulfur groups (Schuster, 1991). When normalized to Rb, the Hg/Rb profile (SI.4) shows stable values from the bottom of the core up to 47 cm deep (~ AD 1921) followed by a gradual increase by a factor 5 around 34 cm depth, demonstrating an increased atmospheric input from ~ 1920 to in the early 1950's. During the detrital period (47 to 37 cm), Hg, Br and S show an inverse trend with Rb or Ti (Fig. 3 and S.I. 4) suggesting that detrital inputs were dominantly composed of inorganic constituents with low Hg contents. This would dilute atmospheric Hg inputs to the Lake as it is partly associated with OM resulting from the degradation of the surrounding vegetation. Then, the Hg/Rb ratios slightly decrease from 34 cm depth to the top of the core. Both Pb and Hg normalizations to terrigenous proxies highlight the importance of atmospheric anthropogenic inputs to the lake which largely dominate those from the watershed since the beginning of World War I.

3.3. Tracking Hg sources using isotopic composition

In our data set, significant MDF (within a 0.6 ‰ range for δ^{202}Hg) and MIF (within a 0.6 ‰ range for both Δ^{201}Hg and Δ^{199}Hg) signatures were observed (S.I. 5 and Figure 4). Δ^{200}Hg were close to zero (S.I.5) and correlated as expected from the theoretical line.

We reported in the previous section that most of the Hg inputs originated from the atmospheric compartment. Indeed, owing to the peat type vegetation (i.e., Sphagnum mosses)

which encircles Lake Luitel and acts as a physical barrier for particles, the terrigenous Hg contribution may be negligible or strongly diluted (e.g., during the detrital event) since our sediment values (mean ± 2SD; δ^{202}Hg: -1.14 ± 0.31 ‰; Δ^{199}Hg: -0.22 ± 0.22 ‰) are far from the available reported data for crust values (δ^{202}Hg = -0.6 to -0.1 and Δ^{199}Hg close to zero) (Smith et al., 2008) or for Mt Leigong bedrock (δ^{202}Hg: -0.92 to -0.86; Δ^{199}Hg: -0.04 to +0.01 ‰) (Zhang et al., 2013). In addition, the isotopic signature of our data set is relatively close to those reported for the organic surface soil layers of a pristine Wisconsin forest (δ^{202}Hg: -1.88 to -1.22 ‰; Δ^{199}Hg: -0.22 to -0.14 ‰) (Demers et al., 2013) and those for lichens from urban, suburban and rural areas (δ^{202}Hg: -1.27 to -0.95 ‰; Δ^{199}Hg: -0.39 to -0.28 ‰) (Enrico et al., 2013; Estrade et al., 2010). Based on this assumption, both uptake of atmospheric Hg by surrounding vegetation and direct atmospheric deposition (which are enriched in heavier isotopes (Gratz et al., 2010; Rolison et al., 2013; Sherman et al., 2010)) are the likely major processes for Hg incorporation in the lake. Indeed, plant leaves, lichens and mosses have been reported to uptake isotopically lighter atmospheric Hg (Demers et al., 2013; Yin et al., 2013), while their decomposition has been suggested to generate no significant changes in the Hg isotopic composition (Demers et al., 2013).

To estimate Hg pollution sources in the ecosystem, we can use binary mixing models (Figure 4 and S.I.6) which have been successfully used by many authors to discriminate natural and anthropogenic sources. Considering Δ^{199} Hg (or δ^{202}Hg, see S.I. 6) vs 1/AR Hg (or 1/[THg] see S.I. 6) values, three subsets can be distinguished that are dated at (i) before 1920, (ii) between 1946 and 1991 and (iii) after 1991. In comparison with numerous studies that used concentrations rather than accumulation rates, the coupling of Δ^{199} Hg with Hg AR enables comparison of Hg fingerprints with the integrated temporal information of the reservoir mixing in the sediment (i.e., lithogenic and atmospheric). Samples from before 1920 were already affected by anthropogenic sources since 1/[THg] or 1/Hg AR data ranged between

reported values for pre-industrial/background and recent contaminated sediments (Biester et al., 2007; Mil-Homens et al., 2013; Sonke et al., 2010). Samples from after 1920 show the typical 1/[THg] range of value measured in industrial contaminated sediments (Biester et al., 2000; Cossa and Martin, 1991; Garcia Bravo et al., 2011; Guédron et al., 2011; Guédron et al., 2012; Liu et al., 2012; Mil-Homens et al., 2013; Monperrus et al., 2007). Most dramatically, the sample set dated from 1923 to 1991 have the lowest 1/[THg] or 1/Hg AR data with the less negative Δ^{199} Hg being typical of an industrial signature. Then, the sample set dated after 1991 shows intermediate values in relation to the two previous sets.

The strong correlation between Δ^{199}Hg and 1/Hg AR (r^2 = 0.755, P < 0.01, Fig. 4a) is the main feature of our archive record; this highlights that the MIF signature seems to be a combined signature of all local Hg sources although Lake Luitel receives atmospheric Hg from various industrial sources. Such correlation also reveals that industrial end-members have less negative MIF signatures that are close to those reported for smelter dust (Bigham et al., 2013) or sediments contaminated by smelter emissions (Gray et al., 2013) and sediments contaminated by industry and chlor-alkali plants emissions (Mil-Homens et al., 2013; Perrot et al., 2010). This is in accordance with the main probable sources of Hg emission identified in the area of Lake Luitel (Fig. 1) which are, with respect to their increasing distance to the lake; (i) the ferrous and non-ferrous (electro-)metallurgy from the Livet-Gavet area, (ii) the chemical complex of South Grenoble (Pont de Claix and Jarrie chlor-alkali plant) and (iii) the cement factories in western Grenoble (Fig. 1). Since industrial emissions from the various sources were either not continuous or varied strongly in intensity throughout history, our data set shows that the MIF signature makes Hg isotopic fingerprinting unable to discriminate industrial sources.

Besides, the plot of δ^{202}Hg vs Δ^{199} Hg isotope values and its comparison with literature data (Fig. 4b) enabled us to refine the potential sources and incorporation pathways of Hg in Lake

Luitel. This plot also enables us to identify the three previous main subsets with some outliers (i.e., the samples dated from the two world wars and interwar period) that are spread within the three subset domains.

Firstly, samples dating before 1920 have the lowest δ^{202}Hg (-1.30 ± 0.23 ‰) and Δ^{199} Hg (-0.43 ± 0.11 ‰) signatures, which are similar to those reported from sediments dated from the early 1900's (i.e., industrial revolution period: δ^{202}Hg: -1.27 to -2.29 ‰; Δ^{199}Hg: -0.20 to -0.35 ‰) (Gray et al., 2013) or sediments defined as background sediments (δ^{202}Hg: -1.00 ± 0.19 ‰; Δ^{199}Hg: -0.20 ± 0.11 ‰) (Sonke et al., 2010) and those for lichens from suburban and rural areas (δ^{202}Hg: -1.27 to -1.00 ‰; Δ^{199}Hg: -0.39 to -0.50 ‰) (Estrade et al., 2010). These Hg isotopic signatures suggest that Hg sources to the lake prior to 1920 were dominated by a global atmospheric background Hg signature with a moderate anthropogenic influence.

Secondly, samples dated from 1946 to 1991 have a slightly heavier range of δ^{202}Hg (-1.12 ± 0.27 ‰) but the less negative values of Δ^{199}Hg (-0.15 ± 0.04 ‰) and Δ^{201}Hg (-0.17 ± 0.06 ‰). These signatures correspond to values reported for sediments contaminated by a chlor-alkali plant (Δ^{199} Hg: □ 0.04 ± 0.15 ‰; Δ^{201} Hg: □ 0.02 ± 0.09 ‰) (Perrot et al., 2010) or Pb-Zn smelter dust (Δ^{199} Hg: □ 0.13 to -0.01 ‰; Δ^{201} Hg: □ 0.11 to 0.06 ‰) (Estrade et al., 2011) and for lichens collected in the vicinity of urban and industrial sites (Estrade et al., 2010; Estrade et al., 2011). Such a shift to values close to zero Δ^{199}Hg with the increase of THg concentrations in the sediment is indicative of the rising contribution of anthropogenic Hg sources.

Thirdly, the sample set dated from the most recent period (1998 to 2011), have similar δ^{202}Hg (-1.15 ± 0.30 ‰) as the previous period but the Δ^{199}Hg (□ 0.26 ± 0.07 ‰) returns to more negative MIF values suggesting a reduction of industrial emissions to the lake with a change in emission sources being dominated by urban type emission. Finally, the outlier data set

dated during the world wars and interwar period (1916 to 1946) have the largest range of δ^{202}Hg (-1.02 ± 0.35 ‰) and Δ^{199}Hg (-0.23 ± 0.19 ‰) which are spread within the two later data sets, reflecting the important variations of anthropogenic activities during these historical periods.

The absence of a significant correlation between δ^{202}Hg and 1/[THg] (S.I. 6) highlights the caveats that have to be considered using these models since Hg stable isotopes may undergo fractionation from natural and anthropogenic sources and during Hg incorporation in sediment.

In the case of early diagenesis, very little information is available. Up to date, we only know that Hg isotope composition is preserved during OM mineralization in soils under oxic conditions (Demers et al., 2013). This may not be the case of diagenetic processes occurring under sub- to anoxic conditions. In the case of Lake Luitel's organic sediment, where the sedimentation rate and total Hg concentrations are high, we can hypothesize that, although changes in speciation occur during diagenetic processes, the bulk isotopic ratio may be preserved. Besides, Hg isotope fractionation can also result as a function of the distance and intensity of the sources with an eventual enrichment in light isotopes with increasing distance. Owing to the lack of Hg isotopic data available for the numerous local Hg sources (i.e., ferrous and non-ferrous ores, La Mure coal, incinerator smokes and chloralkali) it is hard to apportion the Hg fluxes and signatures originating for each of them. In addition, the complexity of wind directions between the valleys and the seasonal thermic inversion (during the winter) render difficult the physical decoupling in terms of atmospheric transfer in relation to distances to the sources (Chemel et al., 2005; Milhe et al., 1971; Mimeau, 2013).

3.4. Historical reconstruction of mercury accumulation rates from industrial sources

3.4.1. Industrial revolution period (1860-1910)

Mercury accumulation rates (Hg AR) in the period 1860 □ 1915 remain constant (~ 45 µg.m^{-2}.y^{-1}, Fig. 5) and in the range of reported Hg AR for the early-industrial period (Thevenon et al., 2011). This period corresponds to the emergence of hydroelectricity in the Alps with rising needs for steel for the construction of power stations. Therefore, the demand for iron and coal increased progressively and local mining activities rose in the surrounding Romanche and Oisan valleys (mainly iron), in the city of la Mure (largest anthracite mine), as well as metallurgical activities in the Romanche valley and Belledonne mountains (e.g., Rioupéroux and Allevard – Figure 1) (CPI, 2007). To a lesser extent, cement (Avenier, 2004) and lime production, located in the Chartreuse and Vercors mountains (CPI, 2007), also led to significant Hg emissions due to wood and coal consumption for kilns and ore burning. This accounts for higher Hg AR values in the industrial revolution period compared to the pre-industrial period (1 □ 4 µg.m^{-2}.y^{-1} (Biester et al., 2007)). However, these Hg ARs remain moderate in comparison to the modern industrial period. Indeed, the Hg isotopic signature (i.e., most negative δ^{202}Hg and Δ^{199}Hg values) recorded before World War I (WWI, 1914 – 1918) was in the range of reported signatures for background sediments and lichens of suburban and rural areas. Although our record cannot provide Hg isotopic signatures typical of the pre-industrial period (prior to 1860), these observations suggests that Lake Luitel sediment has recorded a signature dominated by global Hg background including a component of the local industrial sources from the surrounding valleys (Sun et al., 2016).

3.4.2. WWI, WWII and the interwar period

During WWI, the Hg accumulation rate increased by a factor two (Fig. 5). At this time, the Grenoble valley (Jarrie and Pont de Claix) was one of the three most important chemical industry sites in France for the production of smoke bombs (stannous tetrachloride) and combat gases (phosgene and yperite) (CPI, 2007). However, all chloride derivate products

were produced with membrane cells without Hg use. The Grenoble region was also a huge shell producer and at the height of the conflict around 50,000 shells were produced per day (Blanchard, 1916). Such production implied an increase of metallurgical activities as well as coal (anthracite from La Mure mine) production and combustion for the supply of furnaces. All these activities are the most likely sources of Hg emissions to the atmosphere during WWI. Both MIF and MDF signatures of Hg for WWI remained similar to the previous period.

Between WWI and WWII, Hg AR stabilized around 150 µg m^{-2} y^{-1}, indicative of (i) the reconversion of the industry from military to civilian activities (e.g., production of chlorine derivatives) by the chemical industry complex and (ii) the 1929 economic crisis which slowed down several sectors of regional industry (CPI, 2007). Although this interwar period corresponds to the detrital period (1921 -1939), the observed gradual shift of both the Δ^{199} Hg and δ^{202}Hg signature to less negative values testifies to an increased anthropogenic signature. Therefore, the terrigenous Hg inputs likely had little influence in comparison to anthropogenic ones (see section 3.2) and their associated signatures have been diluted by the later. Indeed, this shift coincides with the sharp increase of Ferro-manganese production in the surrounding Clavaux factories (Fig. 5) which used electric furnaces for metallurgical operations due to the easy access to hydroelectricity from power plants installed in the Romanche river (Giandou, 2000). This recorded enrichment in heavier δ^{202}Hg isotopes also corresponds to the reported values for smelter dust (Estrade et al., 2011) and sediment contaminated by smelter emissions (Gray et al., 2013). The absence of fuel in the (electro)smelting process suggests that the Hg signature from these smelting-derived atmospheric emissions may derivate from the Hg initially present in the ores. Indeed, reported δ^{202}Hg from various deposits worldwide (Foucher et al., 2009; Gray et al., 2013; Sonke et al., 2010; Stetson et al., 2009) are similar to the δ^{202}Hg values recorded during this interwar

period. In addition, the corresponding MIF values are in accordance with previous studies that reported slightly negative MIF values (Gratz et al., 2010; Sherman et al., 2010) in Hg liberated (mostly gaseous elemental Hg: GEM) at high temperature during industrial processes (Estrade, 2010).

The World War II (WWII: 1939 – 1945) period is characterized by a sharp increase of Hg AR, with a maximum value around 250 µg m^{-2} y^{-1} followed by a decrease from 1945 until the mid-1950's down to 170 µg m^{-2} y^{-1} due to the post war decreased activity in all industrial sectors. During WWII, as for WWI, the demand for chemical and metallurgical products rose sharply. Most of the local industry was involved in the "war effort", as for example the paper factories which changed their activities to bomb assembly and production (Spillmaecker et al., 2009). The huge increase in metallurgical (mostly to satisfy weapon industry demand) and chemical (i.e., chemicals production, electrochemistry and electrometallurgy) activities lead to increased atmospheric Hg emission, via e.g. coal and wood combustion, although the relative contribution amongst these numerous industrial activities is poorly documented. During this period, the Δ^{199} Hg signature continued to decrease to reach less negative values at the end of the war, highlighting the continuous increase of anthropogenic emissions during this period. In addition, the Hg MDF signature exhibits a major unconformity around 1942 where δ^{202}Hg sharply shifts to negative values in the range of the industrial revolution period. Such a signature could be related to increased coal combustion since electrometallurgy sharply decreased at this time (e.g. at the Clavaux site - Fig. 5). Based on this hypothesis, the related Hg isotopic signature would likely result in a less negative shift of MDF since Hg isotopic signature recorded in precipitations and sediments contaminated by atmospheric depositions from coal combustion were enriched in light Hg isotopes (Jackson and Muir, 2012; Sherman et al., 2011) due to the emissions of isotopically light gaseous Hg^0 by coal combustion process (Sherman et al., 2011). However, this remains a hypothesis since the Hg isotopic

signature of the Mure mine anthracite is not documented, and most of reported values for coal worldwide have shown Hg isotopic variation as large as 3.5‰ for δ^{202}Hg (-2.68 to 0.75 ‰) (Biswas et al., 2008; Lefticariu et al., 2011; Sun et al., 2013a; Sun et al., 2013b).

After WWII, δ^{202}Hg values return gradually to the less negative values around 1950 coinciding with the maximum Hg AR recorded in our archive and with the reactivation of electrometallurgy sites at the end of WWII (Giandou, 2000).

3.4.3. Modern industry and urban development period (1955 – 1980)

From 1955 to 1960 a slight increase of Hg AR from 170 to 190 µg m^{-2} y^{-1}, reflects the recovery of industrial and economical activities. Then, from 1960 to 1973, Hg AR decreased slightly to stabilize around 145 µg m^{-2} y^{-1}. After the petrol crisis of 1973, Hg AR remained stable at 140 µg m^{-2} y^{-1} until 1990.

The "glorious thirties" period (1950 – 1973), known as the post-war prosperity period where French government centralized economic planning on industrial enhancement, is characterized by the most important urban and industrial development of Grenoble city with the construction of large urban infrastructures (buildings, highways, bridges and incinerators), including those of the Olympic games of 1968, large scientific structures (e.g., ILL, LETI and Synchrotron) and hydroelectric structures (dams and power stations) (Soutif, 2005). This period of urban development corresponds to a period of great cement production around Grenoble. Cement production industry was a great consumer of fossil fuels including coal (Martin, 1999) which reached its optimum period of extraction in the anthracite mines of la Mure (Fig. 5) between 1950 and 1966, rising from 450,000 to 791,000 tons of coal extracted per year (CNRS, 1981; Garnier, 2001).

The period 1953 to 1960 coincides with a second return to more negative δ^{202}Hg while MIF values remained slightly negative. Amongst the multiple Hg sources, including industrial

smelting activities in the Livet Gavet area (e.g., Ferro-chrome optimum production period in Clavaux industry – Fig. 5), and other chemical activities around Jarrie, coal combustion for cemeteries could be a dominant source of Hg for such MDF anomalies since the signature for Hg emissions from ferrous and non-ferrous metallurgical activities are likely to be enriched in heavier isotopes (Gray et al., 2013; Sonke et al., 2010). The following period (1965 to 1990) is characterized by an important increase in metallurgical production in the Livet Gavet area (Fig. 5) and by the installation of 3 chlor-alkali cells between 1957 and 1962 in the chemical factory of Jarrie/Champs sur Drac. This chlor-alkali plant was reported as the main local Hg^0 emitter to the atmosphere (Fig. 5) before other combustion processes (e.g., municipal waste incinerator and municipal heater) (Arnaud, 2004; Dommergue et al., 2002; DRIRE, 2006; Grangeon et al., 2012; Guédron et al., 2013). The $\delta^{202}Hg$ shift to less negative values (~ 1.1 ‰) recorded during this period corresponds to reported $\delta^{202}Hg$ values for chlor-alkali contaminated sediments (Perrot et al., 2010) and is suggestively attributed to evasion of Hg^0 from the chlor-alkali plant combined with the Hg signature of electrometallurgical activities emissions.

3.4.4. The regulation period (1998 – 2011)

From 1990 to 2011 a significant decrease in Hg ARs from ~ 140 to ~ 90 µg m^{-2} y^{-1} coincides with the application of environmental regulations that obliged industrials to reduce atmospheric emissions (Amos et al., 2015) and improve industrial processes (i.e., stack filtration). Among these industrial improvements, the chlor-alkali plant performed several rehabilitation operations in the 1980's to reduce Hg^0 losses and one of the three units was dismantled in 1986 followed by dismantling of the two other ones in 2012. Such operations resulted in reported reductions of about 300 % of Hg^0 emissions from the plant between 2000 and 2004 (Arnaud, 2004; DRIRE, 2006; DRIRE, 2010). However, although Hg^0 emissions

from chlor-alkali were reduced during this period, reported Hg emissions from municipal waste incinerators tended to increase and become major atmospheric sources (Arnaud, 2004; DRIRE, 2006; DRIRE, 2010), according to the great demographic and urban development (INSEE, 2014). At the time, the cement industry converted to alternative fuels with co-combustion of urban waste together with fuel oil or coal, with up to 50 % urban waste used as fuel in 1995 (Martin, 1999). The reduction of Hg AR is accompanied with a slight return to more negative Δ^{199}Hg values around -0.3 ‰. In parallel, another major unconformity in δ^{202}Hg values is observed in 1999 with a sharp shift to less negative values which gradually return to more negative values between 1999 and 2011 (Fig. 5). Such unconformity for δ^{202}Hg values in 1999 may be attributed to (i) a major change in industrial or urban emissions and/or (ii) to a natural event. The most probable reason is the installation in 1996 of 3 new gas incineration devices in the municipal waste incinerator (MWI) of the Grenoble urban conglomeration (Oudot, 2005). This induced an increase in the amount of waste used for combustion, from 100,000 to 166,000 tons between 1994 and 2004 (Oudot, 2005). In the meantime, air pollution control devices (APCD) were installed in the MWI with notably the installation of a new APCD in 2005 which permitted the MWI to respect the reinforced regulation. Such APCD suggestively lead to a return to negative δ^{202}Hg values as evidenced by Estrade (2010) who showed that after the condensation process in a municipal solid waste incinerator equipped with an APCD, Hg^0 emissions from the stack were enriched in lighter isotopes (δ^{202}Hg = -1.41 ± 1.13 ‰). Although we cannot provide any evidence of ash layers or other chemical indication of eruptive events in our record, another possible reason for such δ^{202}Hg unconformity would be the occurrence of eruptive events of the Etna and Stromboli volcanoes which exhibited one of the most intense eruptive activities over the last past 300 year between 1998 and 1999 (almost 120 explosive events) reaching their paroxysm on 22nd July 1998 (Daniele et al., 2009; Quattrocchi et al., 2000). During Etna eruptions, gaseous

atmospheric mercury emissions were reported to be dominated by gaseous Hg^0 emitted over long distances (Bagnato et al., 2007) which are enriched in light isotopes ($\delta^{202}Hg$ = -0,75‰) (Perrot, 2008; Sonke et al., 2008; Zambardi et al., 2009).

4. Conclusion

In this study, we showed that Hg isotopic signature is a relevant and promising tool for the historical reconstruction of anthropogenic Hg emissions and may have potential for identifying their relative contributions. In particular, we highlighted that the Hg MIF reflected a global pool of industrial and urban emissions which tend to shift to less negative MIF values between the period prior to 1920 (-0.43 ± 0.11 ‰) and periods of higher anthropogenic activities (-0.15 ± 0.04 ‰). In addition, MDF signatures enabled identification of two major contributors, i.e., (i) the combustion activities (smelters, cement factories and urban heating) with more negative $\delta^{202}Hg$ values, and (ii) chemical and electrometallurgical activities (electrochemistry, chlor-alkali) with higher $\delta^{202}Hg$ values. Along the studied period, the MDF signature recorded in the sediment varied in relation to the relative intensities of these two major sources. Finally, we showed the efficiency of recent law enforcements aimed at reducing Hg emissions (1998 – 2011) as Hg AR decreased with a return to more negative MIF and MDF signatures tending toward those of the industrial revolution period.

However, this reconstruction would not have been possible without the combination of various other kinds of information, such as chemical, sedimentological and historical data. Especially, the Hg isotopic signature of numerous local sources (e.g., local anthracite) and of the Hg emitted from various combustion or smelting processes using or not combustible (i.e., electro-chemistry vs combustion using various fuels) are amongst the major data needed to better constrain Hg source identification. In addition, the complexity of wind dynamics in the region did not enable the source apportioning of identified Hg sources. Finally, a lack of

knowledge still remains with regard to Hg fractionation during early diagenesis which is crucial to understand MDF during Hg incorporation in the sediment and to better constrain the Hg signature recorded in sediments.

Acknowledgment

We greatly acknowledge the Conseil General de l'Isère for funding and supporting this study, and the ONF (Office National des Forêts) for their help in terms of logistics and access to historical archives of the Lake Luitel. We also thank Chantal Spillemaecker (curator in chief of the Musée dauphinois (Grenoble) and Director of the Musée Hector-Berlioz) and Cédric Avenier for their precious help in the access of historical archives of the industrial past of the studied region. We thank the LSM facilities for gamma spectrometry measurement and EDYTEM for X-ray fluorescence analyses. We finally thank Joel Blum and the anonymous reviewer for their great work in the review process which allowed us to greatly improve the manuscript. Finally, we greatly thank Jennifer Harris-Hellal for the complete English revision of the manuscript.

References

Allan, M. et al., 2013. Reconstructing historical atmospheric mercury deposition in Western Europe using: Misten peat bog cores, Belgium. Science of The Total Environment, 442(0): 290-301.

Amos, H.M. et al., 2015. Observational and modeling constraints on global anthropogenic enrichment of mercury. Environmental science & technology, 49(7): 4036-4047.

Appleby, P. and Oldfield, F., 1978. The calculation of lead-210 dates assuming a constant rate of supply of unsupported 210Pb to the sediment. Catena 5: 1-8.

Arnaud, T., 2004. Cadastre des émissions de mercure sur Grenoble et son agglomération, ASCOPARG, Grenoble.

Avenier, C., 2004. Ciments d'églises, semences de chrétiens: constructions religieuses et industrie cimentière en Isère au XIXème siècle, Grenoble 2.

Bagnato, E. et al., 2007. Degassing of gaseous (elemental and reactive) and particulate mercury from Mount Etna volcano (Southern Italy). Atmospheric Environment, 41(35): 7377-7388.

Bajard, M. et al., 2016, in press. Erosion record in Lake La Thuile sediments evidences montane landscape dynamics through the Holocene. Holocene: doi: 10.1177/0959683615609750

Bergquist, B.A. and Blum, J.D., 2007. Mass-dependent and-independent fractionation of Hg isotopes by photoreduction in aquatic systems. Science, 318(5849): 417-420.

Biester, H., Bindler, R., Martinez-Cortizas, A. and Engstrom, D.R., 2007. Modeling the Past Atmospheric Deposition of Mercury Using Natural Archives. Environ. Sci. Tech., 41(14): 4851-4860.

Biester, H., Gosar, M. and Covelli, S., 2000. Mercury speciation in sediments affected by dumped mining residues in the drainage area of the Idrija mercury mine, Slovenia. Environmental Science & Technology, 34(16): 3330-3336.

Bigham, G., Monte, C. and Pozzi, C., 2013. Using Mercury Isotopic Signatures to Trace Deposition of Steel Plant Atmospheric Emissions in Southern Italy International Conference on Mercury as A Global Pollutant, Edimburg.

Biswas, A., Blum, J.D., Bergquist, B.A., Keeler, G.J. and Xie, Z., 2008. Natural mercury isotope variation in coal deposits and organic soils. Environ. Sci. Technol., 42(22): 8303-8309.

Blanchard, R., 1916. L'état actuel de l'industrie en Dauphiné (région de Grenoble), Recueil des travaux de l'institut de géographie alpine, Grenoble, pp. 329-354.

Blum, J.D. and Bergquist, B.A., 2007. Reporting of variations in the natural isotopic composition of mercury. Analytical and bioanalytical chemistry, 388(2): 353-359.

Blum, J.D., Sherman, L.S. and Johnson, M.W., 2014a. Mercury Isotopes in Earth and Environmental Sciences. Annual Review of Earth and Planetary Sciences, 42(1): 249-269.

Blum, J.D., Sherman, L.S. and Johnson, M.W., 2014b. Mercury isotopes in earth and environmental sciences. Annual Review of Earth and Planetary Sciences, 42: 249-269.

Chemel, C., Chaxel, E., Couach, O. and Chollet, J.P., 2005. Influence of the interactions of local dynamical processes with large-scale flow on air quality in the Grenoble area. Hrvatski meteoroloski casopis, 40(40): 184-187.

CNRS, 1981. La Mure en Matheysine – La volonté de vivre. C.N.R.S. - Université Pierre Mendès France, Grenoble.

Cossa, D. and Gobeil, C., 2000. Mercury speciation in the Lower St. Lawrence estuary. Can. J. Fish. Aquat. Sci., 57: 138-147.

Cossa, D. and Martin, J.-M., 1991. Mercury in the Rhone delta and adjacent marine areas. Marine Chemistry, 36(1â€“4): 291-302.

CPI, 2007. Atlas du patrimoine industriel (in French). Patrimoine en Isère. Conservatoire du Patrimoine de l'Isère / Conseil Général Isère, Grenoble, 145 pp.

Daniele, P., Lirer, L., Petrosino, P., Spinelli, N. and Peterson, R., 2009. Applications of the PUFF model to forecasts of volcanic clouds dispersal from Etna and Vesuvio. Computers & Geosciences, 35(5): 1035-1049.

Demers, J.D., Blum, J.D. and Zak, D.R., 2013. Mercury isotopes in a forested ecosystem: Implications for aira surface exchange dynamics and the global mercury cycle. Global Biogeochemical Cycles, 27: 222-238.

Desplanque, C. and Garambois, S., 2009. Caractérisation de la paléotopographie de la tourbière ombrotrophe du Luitel au moyen de méthodes géophysiques. In: C. Tourbières (Editor), Ann. Sci. Rés. Bios. Trans. ONF Isère et LGIT, Grenoble, Vosges du Nord-Pfälzerwald, pp. 305-315.

Dommergue, A.l., Ferrari, C.P., Planchon, F.d.r.A.M. and Boutron, C.F., 2002. Influence of anthropogenic sources on total gaseous mercury variability in grenoble suburban air (France). Sci. Tot. Environ., 297(1-3): 203-213.

Donovan, P.M., Blum, J.D., Yee, D., Gehrke, G.E. and Singer, M.B., 2014. An isotopic record of mercury in San Francisco Bay sediment. Chemical Geology, 349-350(0): 87-98.

DRIRE, 2006. Bilan de l'environnement industriel en Rhône-Alpes, DRIRE Rhône-Alpes, Grenobe.

DRIRE, 2010. Plan de protection de l'atmosphère de Grenoble 2005-2010, Prefecture de l'ISère, Grenoble.

Elbaz-Poulichet, F., Dezileau, L., Freydier, R., Cossa, D. and Sabatier, P., 2011. A 3500-year record of Hg and Pb contamination in a Mediterranean sedimentary archive (The Pierre Blanche Lagoon, France). Environ. Sci. Tech., 45(20): 8642-8647.

Enrico, M., Heimbürger, L.E., Le Roux, G. and Sonke, J., 2013. A multi-coring approach to assess intra-site variability in atmospheric Hg deposition, and Hg isotopic

composition, to peat bogs Mercury as a global pollutant. Mercury stable isotope biogeochemistry 1, Edimburg.

Estrade, N., 2010. Discrimination et traçage isotopique des sources anthropiques du mercure dans l'environnement. P.h.D Thesis, Université de Pau et des Pays de l'Adour, Pau, 238 pp.

Estrade, N., Carignan, J. and Donard, O.F.X., 2010. Isotope Tracing of Atmospheric Mercury Sources in an Urban Area of Northeastern France. Environmental Science & Technology, 44(16): 6062-6067.

Estrade, N., Carignan, J. and Donard, O.F.X., 2011. Tracing and Quantifying Anthropogenic Mercury Sources in Soils of Northern France Using Isotopic Signatures. Environmental Science & Technology, 45(4): 1235-1242.

Foucher, D. and Hintelmann, H., 2006. High-precision measurement of mercury isotope ratios in sediments using cold-vapor generation multi-collector inductively coupled plasma mass spectrometry. Anal. Bioanal. Chem. , 384(7-8): 1470-1478.

Foucher, D., Ogrinc and Hintelmann, H., 2009. Tracing Mercury Contamination from the Idrija Mining Region (Slovenia) to the Gulf of Trieste Using Hg Isotope Ratio Measurements. Environmental Science & Technology, 43(1): 33-39.

Garcia Bravo, A., Bouchet, S., Amouroux, D., Poté, J. and Dominik, J., 2011. Distribution of Mercury and Organic Matter in Particle-Size Classes in Sediments Contaminated by a Waste Water Treatment Plant: Vidy Bay, Lake Geneva, Switzerland. J. Environ. Monit., 13: 974-982.

Garnier, J., 2001. Chronique des Mines de La Mure – 2 siècles de charbon. Garnier.

Gehrke, G.E., Blum, J.D. and Meyers, P.A., 2009. The geochemical behavior and isotopic composition of Hg in a mid-Pleistocene western Mediterranean sapropel. Geochimica et Cosmochimica Acta, 73(6): 1651-1665.

Giandou, A., 2000. Les Clavaux du carbure de calcium au silicium. Histoire Industrielle. Presses Universitaires de Grenoble, Grenoble, 152 pp.

Golberg, E., 1963. Geochronology with 210Pb, Radioactive Dating. International Atomic Energy Agency, Vienna, pp. 121-131.

Grangeon, S., Guédron, S., Asta, J., Sarret, G. and Charlet, L., 2012. Lichen and soil as indicators of an atmospheric mercury contamination in the vicinity of a chlor-alkali plant (Grenoble, France). Ecol. Indic., 13(1): 178-183.

Gratz, L.E., Keeler, G.J., Blum, J.D. and Sherman, L.S., 2010. Isotopic Composition and Fractionation of Mercury in Great Lakes Precipitation and Ambient Air. Environmental Science & Technology, 44(20): 7764-7770.

Gray, J.E., Pribil, M.J., Van Metre, P.C., Borrok, D.M. and Thapalia, A., 2013. Identification of contamination in a lake sediment core using Hg and Pb isotopic compositions, Lake Ballinger, Washington, USA. Applied Geochemistry, 29: 1-12.

Guédron, S., Cossa, D., Grimaldi, M. and Charlet, L., 2011. Methylmercury in tailings ponds of Amazonian gold mines (French Guiana): Field observations and an experimental flocculation method for in situ remediation. Appl. Geochem., 26(2): 222-229.

Guédron, S., Grangeon, S., Jouravel, G., Charlet, L. and Sarret, G., 2013. Atmospheric mercury incorporation in soils of an area impacted by a chlor-alkali plant (Grenoble, France): Contribution of canopy uptake. Sci. Tot. Environ., 445-446(0): 356-364.

Guédron, S., Grangeon, S., Lanson, B. and Grimaldi, M., 2009. Mercury speciation in a tropical soil association; Consequence of gold mining on Hg distribution in French Guiana. Geoderma, 153: 331-346.

Guédron, S., Grimaldi, C., Chauvel, C., Spadini, C. and Grimaldi, M., 2006. Weathering versus atmospheric contributions to mercury concentrations in French Guiana soils. Appl. Geochem., 21: 2010-2022.

Guédron, S. et al., 2012. Tidal cycling of mercury and methylmercury between sediments and water column in the Venice Lagoon (Italy). Mar. Chem., 130-131(0): 1-11.

INSEE, 2014. Recensement de la population - Agglo Grenoble Alpes Métropole-Alpes du Sud Isère-Grésivaudan (CT8A) - Évolution de la population depuis 1982. Institut National de la Statistique et des études économiques, Paris, pp. - Agglo Grenoble Alpes Métropole-Alpes du Sud Isère-Grésivaudan (CT8A) - Évolution de la population depuis 1982.

Jackson, T.A., Muir, D.C. and Vincent, W.F., 2004. Historical variations in the stable isotope composition of mercury in Arctic lake sediments. Environ. Sci. Technol. , 38(10): 2813-2821.

Jackson, T.A. and Muir, D.C.G., 2012. Mass-dependent and mass-independent variations in the isotope composition of mercury in a sediment core from a lake polluted by emissions from the combustion of coal. Science of The Total Environment, 417: 189-203.

Klaminder, J., Appleby, P., Crook, P. and Renberg, I., 2012. Post-deposition diffusion of 137Cs in lake sediment: Implications for radiocaesium dating. Sedimentology, 59: 2259-2267.

Krishnaswamy, S., Lal, D., Martin, J.M. and Meybeck, M., 1971. Geochronology of lake sediments. Earth and Planet. Sci. Lett., 11: 407-414.

Lamborg, C.H. et al., 2002. Modern and historic atmospheric mercury fluxes in both hemispheres: Global and regional mercury cycling implications. Global Biogeochem. Cy., 16(4).

Lauretta, D.S., Klaue, B., Blum, J.D. and Buseck, P.R., 2001. Mercury abundances and isotopic compositions in the Murchison (CM) and Allende (CV) carbonaceous chondrites. Geochimica et Cosmochimica Acta, 65(16): 2807-2818.

Lefticariu, L., Blum, J.D. and Gleason, J.D., 2011. Mercury Isotopic Evidence for Multiple Mercury Sources in Coal from the Illinois Basin. Environmental Science & Technology, 45(4): 1724-1729.

Liu, B. et al., 2012. Insights into low fish mercury bioaccumulation in a mercury-contaminated reservoir, Guizhou, China. Environ. Poll., 160(0): 109-117.

Ma, J., Hintelmann, H., Kirk, J.L. and Muir, D.C., 2013. Mercury concentrations and mercury isotope composition in lake sediment cores. Chemical Geology, 366: 96-102.

Martin, J., 1999. Location and Corporate Structure: The Case of the French Cement Industry, 54. London school of economics, London, 32 pp.

Mil-Homens, M. et al., 2013. Tracing anthropogenic Hg and Pb input using stable Hg and Pb isotope ratios in sediments of the central Portuguese Margin. Chemical Geology, 336: 62-71.

Milhe, M., Belle, P. and Vadot, L., 1971. Etude de la dynamique atmosphérique de la région grenobloise en vue de l'application à la diffusion des Polluants. Revue de géographie alpine, 59(3): 283-324.

Mimeau, L., 2013. Suivi environnemental de la Réserve du Luitel. Traitement des données climatiques et modélisation de la nappe de la tourbière du col, LTHE, Grenoble.

Monperrus, M. et al., 2007. The biogeochemistry of mercury at the sediment-water interface in the Thau Lagoon. 2. Evaluation of mercury methylation potential in both surface sediment and the water column. Estuarine, Coastal and Shelf Science. Biogeochemical and contaminant cycling in sediments from a human-impacted coastal lagoon, 72(3): 485-496.

Oudot, C., 2005. Conception du programme de surveillance environnementale autour de l'incinerateur d'ordures ménagères de la Tronche (38), Ecole Nationale de la Santé Publique, Rennes, 70 pp.

Perrot, V., 2008. Géochimie du mercure sur des volcans en dégazage ouvert (Etna, Sicile) et dégazage passif (Merapi, Indonésie): Transport, flux et fractionnement isotopique, University Paul Sabatier, Toulouse, 31 pp.

Perrot, V. et al., 2010. Tracing Sources and Bioaccumulation of Mercury in Fish of Lake Baikal Angara River Using Hg Isotopic Composition. Environmental Science & Technology, 44(21): 8030-8037.

Quattrocchi, F. et al., 2000. Geochemical Monitoring System II prototype (GMS II) installation at the "Acqua Difesa" well, within the Etna region: first data during the 1999 volcanic crisis. Journal of Volcanology and Geothermal Research, 101(3-4): 273-306.

Reyss, J.L., Schimdt, S., Legeleux, F. and Bonte, P., 1995. Large low background well type detectors for measurements of environmental radioactivity. Nuclear Instruments and Methods in Physics Research B(357): 391-397.

Richter, T.O. et al., 2006. The Avaatech XRF Core Scanner: technical description and applications to NE Atlantic sediments. In: R.G. Rothwell (Editor), New Techniques in Sediment Core Analysis. Geological Society, London, pp. 39-50.

Robbins, J. and Edgington, D., 1975. Determination of recent sedimentation rates in Lake Michigan using Pb-210 and Cs-137. Geochim. Cosmochim. Acta, 39: 285-304.

Rolison, J.M., Landing, W.M., Luke, W., Cohen, M. and Salters, V.J.M., 2013. Isotopic composition of species-specific atmospheric Hg in a coastal environment. Chemical Geology, 336: 37-49.

Roos-Barraclough, F. et al., 2002a. An analytical protocol for determination of total mercury concentration in solid peat samples. Sci. Tot. Environ., 292: 129-139.

Roos-Barraclough, F., Martinez-Cortizas, A., Garcia-Rodeja, E. and Shotyk, W., 2002b. A 14 500 year record of the accumulation of atmospheric mercury in peat: volcanic signals,

anthropogenic influences and a correlation to bromine accumulation. Earth and Planetary Science Letters, 202(2): 435-451.

Sabatier, P., Dezileau, L., Briqueu, L., Colin, C. and Siani, G., 2010. Clay minerals and geochemistry record from northwest Mediterranean coastal lagoon sequence: Implications for paleostorm reconstruction. Sedimentary Geology, 228(3-4): 205-217.

Schuster, E., 1991. The behavior of mercury in the soil with special emphasis on complexation and adsorption processes- a review of the literature. Water Air Soil Poll., 56: 667-680.

Sherman, L.S. et al., 2010. Mass-independent fractionation of mercury isotopes in Arctic snow driven by sunlight. Nature Geoscience, 3(3): 173-177.

Sherman, L.S., Blum, J.D., Keeler, G.J., Demers, J.D. and Dvonch, J.T., 2011. Investigation of Local Mercury Deposition from a Coal-Fired Power Plant Using Mercury Isotopes. Environmental Science & Technology, 46(1): 382-390.

Smith, C.N., Kesler, S.E., Blum, J.D. and Rytuba, J.J., 2008. Isotope geochemistry of mercury in source rocks, mineral deposits and spring deposits of the California Coast Ranges, USA. Earth and Planetary Science Letters, 269(3): 399-407.

Sonke, J.E., 2011. A global model of mass independent mercury stable isotope fractionation. Geochimica et Cosmochimica Acta, 75(16): 4577-4590.

Sonke, J.E. et al., 2010. Sedimentary mercury stable isotope records of atmospheric and riverine pollution from two major European heavy metal refineries. Chemical Geology, 279(3): 90-100.

Sonke, J.E., Zambardi, T. and Toutain, J.-P., 2008. Indirect gold trap-MC-ICP-MS coupling for Hg stable isotope analysis using a syringe injection interface. Journal of Analytical Atomic Spectrometry, 23(4): 569-573.

Soutif, M., 2005. Grenoble, carrefour des sciences et de l'industrie. Les Patrimoines, 46. Dauphiné libéré, Grenoble, 51 pp.

Spillmaecker, C. et al., 2009. Papetiers des Alpes (in French). Siècles d'Histoire, 1. Musée Dauphinois, Grenoble, 162 pp.

Stetson, S.J., Gray, J.E., Wanty, R.B. and Macalady, D.L., 2009. Isotopic Variability of Mercury in Ore, Mine-Waste Calcine, and Leachates of Mine-Waste Calcine from Areas Mined for Mercury. Environmental Science & Technology, 43(19): 7331-7336.

Sun, R. et al., 2013a. Mercury stable isotope fractionation in six utility boilers of two large coal-fired power plants. Chemical Geology, 336: 103-111.

Sun, R., Heimbürger, L.E., Sonke, J. and Guijian, L., 2013b. Mercury stable isotopes in coals and coal-hosted rocks: implications for Hg migration and Hg source identification International Conference on Mercury as a Global Pollutant, Edimburg.

Sun, R. et al., 2016. Historical (1850-2010) mercury stable isotope inventory from anthropogenic sources to the atmosphere. Elem Sci Anth, 4(000091): doi: 10.12952/journal.elementa.000091.

Thevenon, F., Guédron, S., Chiaradia, M., Loizeau, J.-L. and Poté, J., 2011. (Pre-) historic changes in natural and anthropogenic heavy metals deposition inferred from two contrasting Swiss Alpine lakes. Quaternary Science Reviews, 30(1-2): 224-233.

Wiederhold, J.G., 2015. Metal Stable Isotope Signatures as Tracers in Environmental Geochemistry. Environmental science & technology.

Yin, R., Feng, X. and Meng, B., 2013. Stable mercury isotope variation in rice plants (Oryza sativa L.) from the Wanshan mercury mining district, SW China. Environmental Science & Technology, 47(5): 2238-2245.

Zambardi, T., Sonke, J.E., Toutain, J.P., Sortino, F. and Shinohara, H., 2009. Mercury emissions and stable isotopic compositions at Vulcano Island (Italy). Earth and Planetary Science Letters, 277(1): 236-243.

Zhang, H. et al., 2013. Atmospheric mercury inputs in montane soils increase with elevation: evidence from mercury isotope signatures. Scientific reports, 3.

Figure Captions

Figure 1: Map of Grenoble city region with locations of lake Luitel, main current and ancient minings (coal, ferrous and non-ferrous), incinerator and industrial ((electro)metallurgy, cementery, organo & electro - chemistry) sites.

Figure 2: Short-lived radionuclides 210Pbex, and 137Cs activity profile with (a) CFCS model applied to (210Pbex) data, (b) the (137Cs) depth profile, and (c) the age model as constrained with 210Pbex and 137Cs data.

Figure 3: XRF multi-elemental analysis (Rb, Br, Pb and Pb/Rb) and THg concentrations profiles vs. age and depth.

Figure 4: a) Δ^{199} Hg vs 1/ Hg AR (mercury accumulation rate) and b) δ^{202}Hg vs Δ^{199} Hg for lake Luitel samples and literature data for various source of Hg.

Figure 5: Panels from left to right: (i) Hg accumulation rate (AR), (ii) δ^{202}Hg and (iii) Δ^{199}Hg values vs. age in lake Luitel sediments and (iv) production of metallurgical products in Clavaux factories, production of anthracite in la Mure mine and Hg emissions from Jarrie chlor-alkali site.

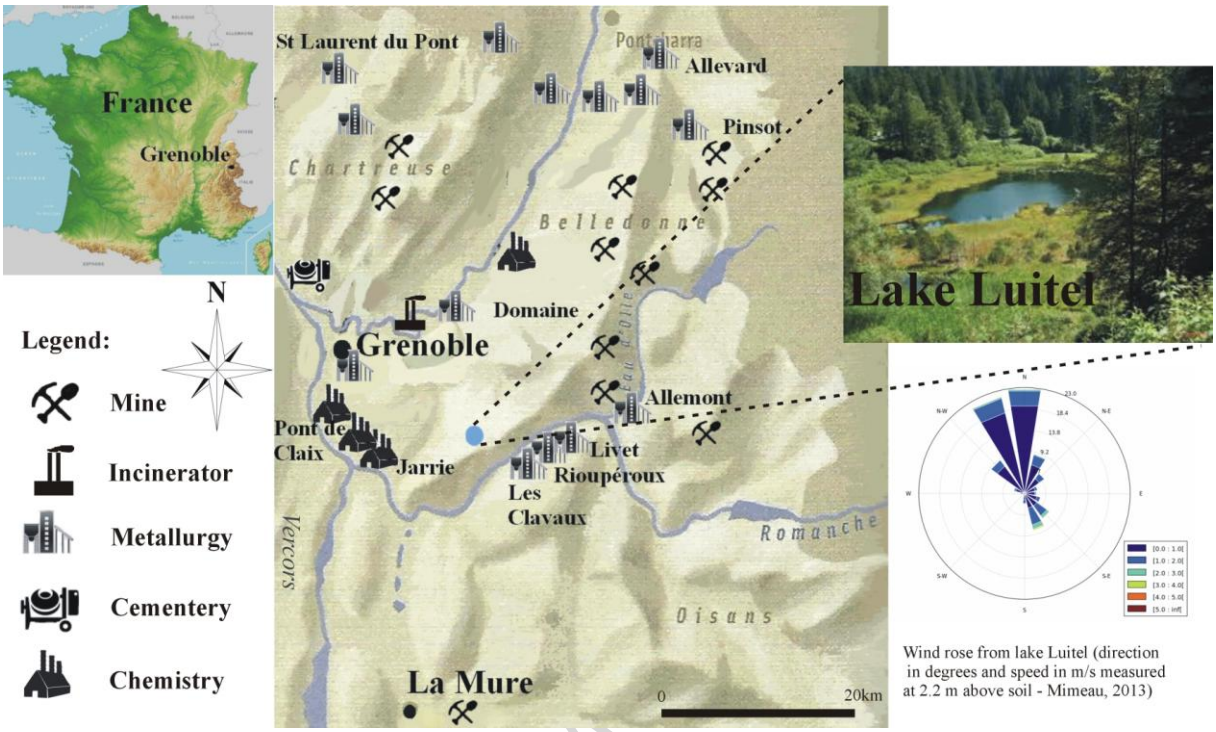

Fig. 1

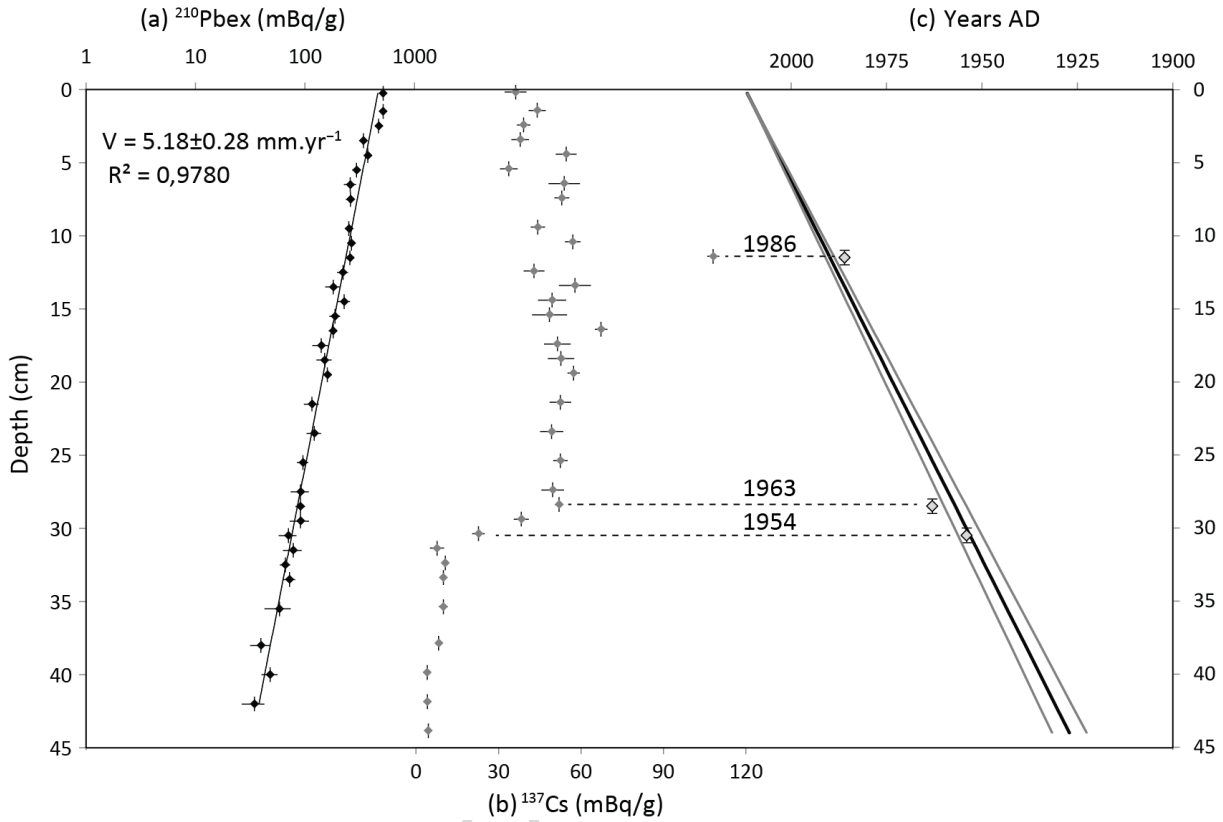

Fig. 2

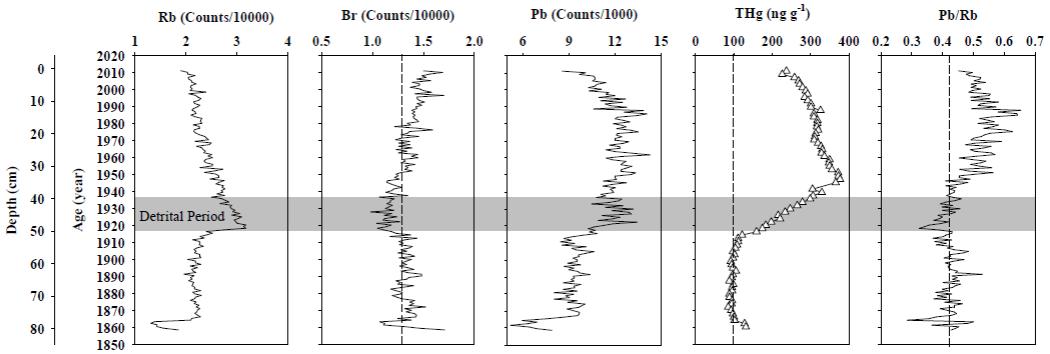

Fig. 3

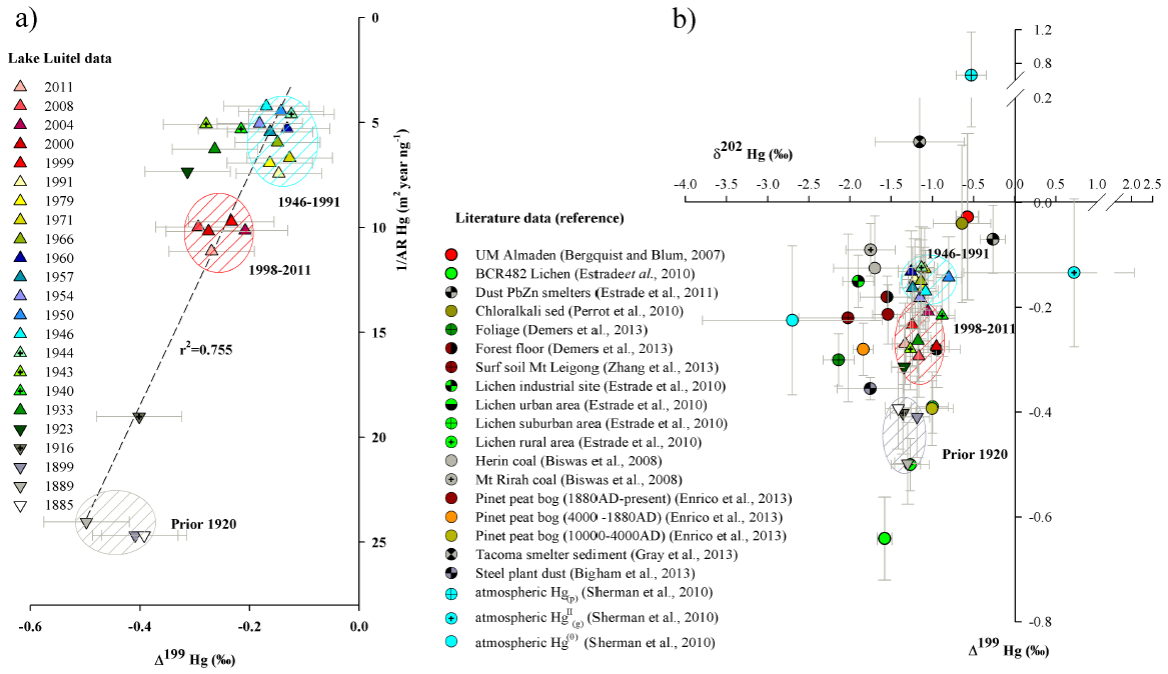

Fig. 4

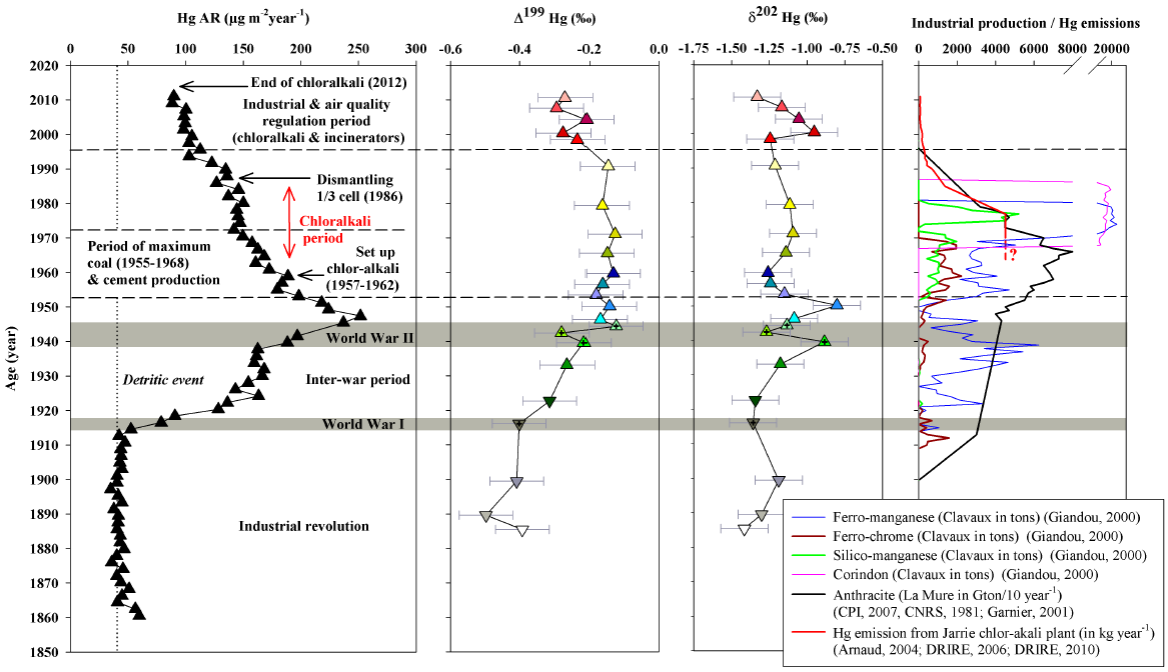

Fig. 5

Research highlights

- We reconstructed industrial and urban mercury (Hg) emissions recorded in the sediment of Lake Luitel over the last 150 year
- We provid a constrained age model with Hg accumulation rates (AR), Hg isotopic composition and exhaustive historical data
- Hg mass independent fractionation (MIF) signature reflect a global pool of industrial and urban emissions
- Hg mass dependent fractionation (MDF) signatures allow the identification of major contributors
- Hg isotopic data combined with historical & chemical data is relevant for the historical reconstruction of Hg emissions